ACCSCIENCE PUBLISHING

Materials Science in Additive Manufacturing

ORIGINAL RESEARCH ARTICLE

Environmental implications of feedback-controlled heat input in wire arc additive manufacturing of Invar 36 through online contact tip-to-workpiece distance adjustment

Elena Manoli[1], Rosa Abate[1], Yushuai Che[2], Luigi Nele[1], Guido Guizzi[1], and Giulio Mattera[1]*

[1]Department of Chemical, Materials and Production Engineering, University of Naples Federico II, Naples, Italy

[2]Department of Management Science and Engineering, Nanjing University of Science and Technology, Nanjing, China

***Corresponding author:** Giulio Mattera (giulio.mattera@unina.it)

Citation: Manoli E, Abate R, Che Y, Nele L, Guizzi G, Mattera G. Environmental implications of feedback-controlled heat input in wire arc additive manufacturing of Invar 36 through online contact tip-to-workpiece distance adjustment. *Mater Sci Add Manuf.* 2026;5(3):026180035. doi: 10.36922/MSAM026180035

Received: April 28, 2026

Revised: May 26, 2026

Accepted: June 7, 2026

Published online: July 8, 2026

Abstract

Wire arc additive manufacturing (WAAM) is attracting increasing interest for the production of large metallic components due to its high material efficiency and productivity. However, process instability and heat input fluctuations can compromise geometric consistency, process reliability, and compliance with qualification requirements, while also affecting energy consumption and environmental performance. This study investigates the environmental implications of feedback-controlled heat-input regulation in WAAM of Invar 36, with particular emphasis on carbon footprint through life cycle assessment (LCA). In contrast to conventional WAAM control strategies, which typically target bead geometry, the proposed approach regulates thermal input through online adjustment of the contact tip-to-workpiece distance (CTWD). This enables heat-input control while preserving the nominal welding parameters, which is particularly relevant for qualification-oriented manufacturing. By combining layer-wise thin-wall experiments with scale-up to an industrial Invar 36 component, the study shows that closed-loop heat-input control increased deposited mass per layer by up to 33.8%, while reducing specific energy consumption and WAAM-only global warming potential (GWP) by up to 25.4% and 25.6%, respectively. At the component scale, the measured energy demand decreased from 8.17 to 7.65 kWh and the WAAM-only GWP from 13.2 to 12.5 kg CO_2-eq. These findings confirm that heat-input regularisation improves WAAM process efficiency and process-related sustainability. However, because feedstock production dominates the total environmental impact, the full carbon-footprint benefit can only be achieved if geometry- or mass-based feedback prevents unnecessary material over-deposition. The results therefore indicate that closed-loop control provides the greatest environmental advantage under equal deposited-mass conditions.

Keywords: Wire arc additive manufacturing; Invar 36; Feedback control; Environmental impact assessment; Life cycle assessment

1. Introduction

In wire arc additive manufacturing (WAAM), feedback control is increasingly recognised as a necessary tool to mitigate the effects of process stochasticity, which can otherwise reduce repeatability, affect geometric accuracy, and compromise deposition stability.[1] Within this framework, heat input is one of the most critical variables to regulate, as it determines the thermal conditions experienced by the build and, consequently, influences bead formation, microstructural evolution, and part quality.[2-5] This issue is particularly relevant in qualification-oriented manufacturing, where maintaining process conditions within prescribed limits is essential to ensure compliance, reproducibility, and confidence in the final component.[6] For this reason, several control strategies have been proposed in the WAAM literature to improve process robustness. Most existing approaches focus on the regulation of geometric features,[7,8] arc stability[9,10] to mitigate layer-wise drift and deposition irregularities. In all these studies, the controlled variables are generally welding speed, wire feed speed, or welding voltage. Recently, increasing attention has been devoted to the control of contact tip to workpiece distance (CTWD) as a means of compensating for the geometrical drift caused by heat accumulation and the resulting layer-wise changes in geometry, especially in thin-walled structures.[11] Moreover, in previous work,[12] it has been demonstrated that CTWD can be effectively used as an actuation variable for heat input regulation, without altering the other qualified process parameters, enabling the automatic compensation of both process drifts and contributing to improved process stability and repeatability.

However, despite the growing interest in process control for WAAM, limited attention has been devoted to the environmental implications of these strategies. This represents an important research gap. A control policy that modifies the process parameters, in order to preserve a target in heat input or layer geometry, may alter not only the geometrical outcome of the build, but also the total deposition time, energy demand, and material efficiency. As a result, the environmental performance of the process may change substantially due to control policies. This is particularly relevant for industrial applications, where the assessment of the final part is increasingly driven not only by quality requirements, but also by environmental performance, reflecting the growing attention paid to sustainable production practices.[13] Within this framework, a growing body of life cycle assessment (LCA) literature has assessed the environmental performance of WAAM, frequently reporting advantages over conventional manufacturing processes due to improved material utilisation and reduced waste generation.[14-17] However, these advantages are strongly case-dependent, and recent evidence suggests that the environmental profile of WAAM may vary substantially with process parameters, energy consumption, component design, and manufacturing configuration.[18] This means that sustainability cannot be regarded as an inherent property of the process alone, but rather as the result of specific operating choices. From this perspective, control strategies deserve explicit investigation, since any action aimed at regulating heat input or geometry may also alter material consumption, deposition time, and electricity demand, thereby influencing the overall environmental outcome of the process.

Motivated by this gap, this paper investigates the environmental implications of feedback-controlled heat input regularisation in the WAAM of Invar 36 alloy. The study moves from previous process-level evidence towards the analysis of a real component, with the aim of understanding how the adoption of this control strategy and the selection of different heat-input setpoints affect energy use, material consumption, and overall environmental impact. In doing so, the paper provides an application-oriented assessment of whether qualification-driven heat input control can also act as a lever for improving the sustainability of WAAM.

2. Materials and methods

2.1. Experimental setup

The experimental setup adopted in this study, as shown in Figure 1, comprises an industrial robotic arm (ABB IRB 2600ID) integrated with an EWM Titan XQ R 400 Puls power source. The robotic system is operated via an IRC5 controller, which communicates with an industrial PC over TCP/IP, enabling the development and implementation of the feedback controller, as briefly described in the following section. Invar 36 wire with a diameter of 1.2 mm was selected as the feedstock material, and its chemical composition is reported in Table 1. Invar 36 is an Fe-Ni alloy containing approximately 36 wt.% Ni, which confers an exceptionally low coefficient of thermal expansion, about $1.94 \cdot 10^{-6} C^{-1}$ also when printed via WAAM.[19] Due to this distinctive property, the alloy is widely used in applications demanding high dimensional stability, including precision instruments, aerospace structures, and cryogenic engineering.

In the aeronautical sector, Invar 36 is commonly employed for the manufacture of tooling used in composite material fabrication processes, such as the industrial-scale component investigated in this study. This alloy has recently attracted attention in WAAM due to its potential for reducing production costs.[20] Indeed, owing to its intrinsic

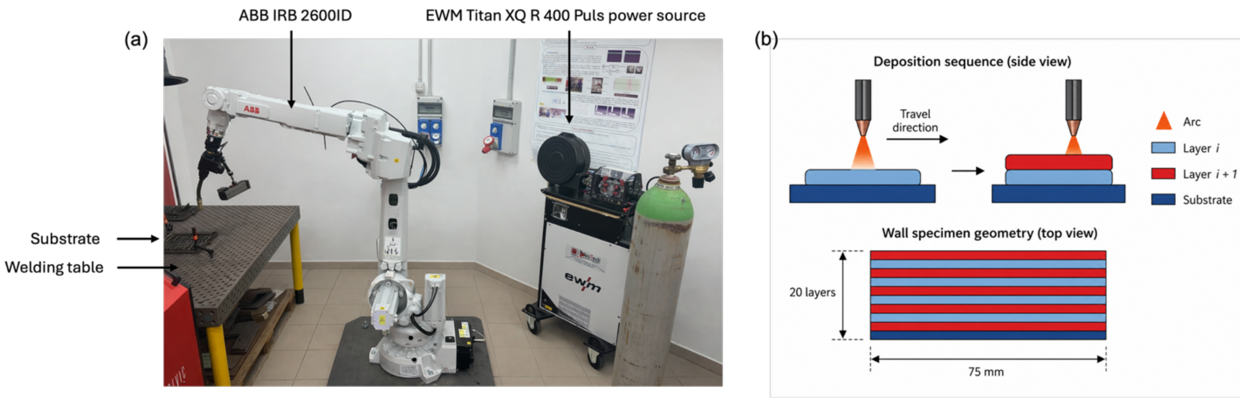

Figure 1. Experimental setup and deposition strategy used for WAAM fabrication of Invar 36 wall specimens. (a) Robotic WAAM system comprising the ABB IRB 2600ID robot, EWM Titan XQ R 400 Puls power source, welding table, and substrate; (b) schematic representation of the layer-wise deposition strategy used to fabricate 20-layer wall specimens over a 75 mm deposition length.

Table 1. Chemical composition (wt%) of the Invar 36 wire (1.2 mm diameter) used in this study

	Fe	Ni	Mn	Si	C	S	P	Ti	Pb
Percentage (%)	63	36	0.3	0.12	0.01	0.004	<0.003	<0.003	0.001

material properties, the alloy is difficult to machine and generally requires multiple processing steps as well as specialised tooling.[21,22] This issue is particularly critical for large-scale components, for which such limitations translate into significantly higher manufacturing costs, further exacerbated by the elevated cost of the raw material itself. Previous studies have demonstrated the feasibility of depositing Invar 36 through several arc-based processes, including gas tungsten arc welding (GTAW),[23] plasma arc welding (PAW),[19,24] and gas metal arc welding (GMAW). More specifically, the literature reports the production of Invar 36 components using both cold metal transfer (CMT)-based modes and conventional short-circuit transfer modes.[25-29] Building on these earlier findings, the optimal process parameters selected in this work were a wire feed speed (WFS) of 6 m/min, a welding voltage (V) of 20V, a welding speed (WS) of 7.5 mm/s, an argon shielding gas flow rate of 12.5 L/min, and a CTWD of 13 mm. According to previous results, these conditions offered the best trade-off between environmental sustainability, with an expected global warming potential (GWP) of 1.52 kg CO_2-eq/kg,[18] and process stability, with a coefficient of variation (CoV) of 16%.[29] Sensors were integrated into the experimental setup to acquire welding current and voltage signals at a sampling frequency of 5 kHz using an NI USB-6361 data acquisition (DAQ) system, which was interfaced with the industrial PC via the NI-DAQmx Python library.

2.2. Feedback control strategy

In previous work, a novel feedback controller, denoted as CCHR (control for heat-input regulation), was introduced.[12] The controller enables real-time adjustment of the CTWD in order to track a target heat input. This approach is grounded in the established relationship between CTWD, arc length, and heat input, as shown in Figure 2. Under constant process conditions, arc behaviour indicates that increasing CTWD results in a reduction in heat input, primarily due to the associated decrease in welding current. Heat input is calculated according to **Equation 1**, where WS is the welding speed, V is the welding voltage, I is the welding current, and η is the arc efficiency, assumed equal to 0.9 within the typical range of 0.85–0.95.

$$H = \eta \cdot \frac{I \cdot V}{WS} \tag{1}$$

The control architecture consists of a combined feedforward and proportional feedback strategy. The feedforward action is obtained through dynamic inversion, whereas the feedback loop is implemented using a proportional controller with gain $k_p = -0.08$. The feedforward term is derived from a step response experiment, in which the CTWD is varied from 11 mm to 17 mm. In this case, the data are acquired and downsampled

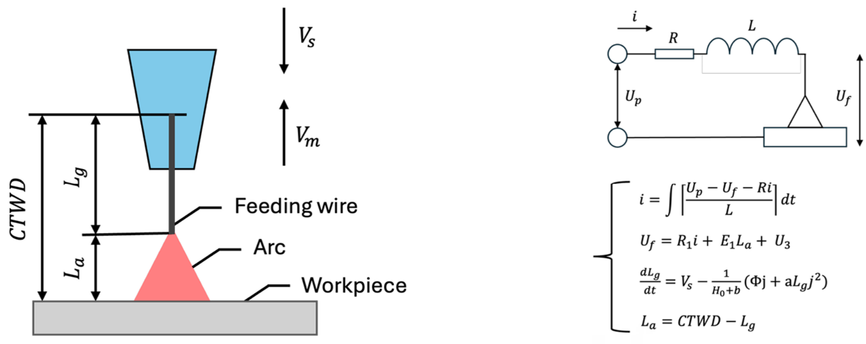

(a) (b)

Figure 2. Effect of CTWD variation on heat input: (a) Response of the main system variables; (b) corresponding RL circuit representation [30,31]

from 5 kHz to a low-frequency representation at 1 Hz for the purpose of modelling the system dynamics, as the controller operates at intervals of 1 s. This choice mitigates the influence of high-frequency spikes associated with the short-circuit transfer behaviour of the arc, thereby enabling the analysis to focus on the slower thermal dynamics driven by heat input. In this context, the average heat supplied is the relevant quantity, rather than its instantaneous variations.

A second-order model is fitted to the observed dynamics (see Figure 3 and **Equation 2**), enabling the identification of the static gain $K = \frac{\Delta H}{\Delta CTWD} = 6.96$. Based on this model and a target heat input, the initial CTWD, namely $CTWD_{ref}$, is computed using **Equation 3**. The feedback controller operates online, using the heat input estimated from the sensor signals and the actual robot speed.

$$G(s) = \frac{K\omega_n^2}{s^2 + 2\zeta\omega_n s + \omega_n^2} = -\frac{47.05}{s^2 + 2.34s + 6.76} \quad (2)$$

$$CTWD_{ref} = CTWD_0 + \frac{H_{ref} - H_0}{K} = 11 - \frac{H_{ref} - 420.2}{6.96} mm \quad (3)$$

In standard open-loop operation, the torch height is increased by a fixed increment corresponding to the average layer height, which is 2.2 mm from previous experiments. In the proposed closed-loop configuration, the CTWD is instead continuously adjusted, allowing for real-time heat input regulation as well as compensation for layer geometry deviations, which accumulate during the building process.[32] An illustrative representation of the proposed controller is shown in Figure 4.

2.3. Data collection procedure

As introduced earlier, the objective of this study is to evaluate the influence of a feedback control loop on the sustainability-related performance of WAAM specimens. For this purpose, structures produced with and without heat input control were compared in terms of material consumption, electrical energy consumption, and argon usage.

Thin-walled specimens were selected for the analysis, consisting of 20 deposited layers over a length of 75 mm. For each test, the target heat input was first defined, after which the feedforward term was computed from the identified process dynamics to determine the initial CTWD. The deposition then proceeded layer by layer by increasing the torch height according to the estimated average layer height of 2.2 mm.

Starting from this common procedure, the process was performed either in open loop, without feedback regulation, or in closed loop, with the heat input controller enabled. In the closed-loop configuration, the CTWD was continuously adjusted online in order to track the prescribed heat input. Three heat input setpoints were considered, namely 340, 380, and 400 J/mm, so as to evaluate the effect of the proposed control strategy under different operating conditions.

The electrical energy consumption was evaluated from the sensor data acquired during the deposition process. Consistently with previous work, the contribution of the robotic system was neglected, since it was markedly lower than that of the welding power source. Therefore, for each deposited layer, the consumption of feedstock material, argon, and electrical energy was quantified and subsequently used for the environmental analysis. More specifically, argon consumption was calculated as the product of the shielding gas flow rate and the welding time. As the gas flow rate was kept constant throughout all tests, the corresponding argon consumption per layer was also constant and equal to 0.0035 kg. Electrical energy consumption was estimated from the average power recorded during deposition and the corresponding

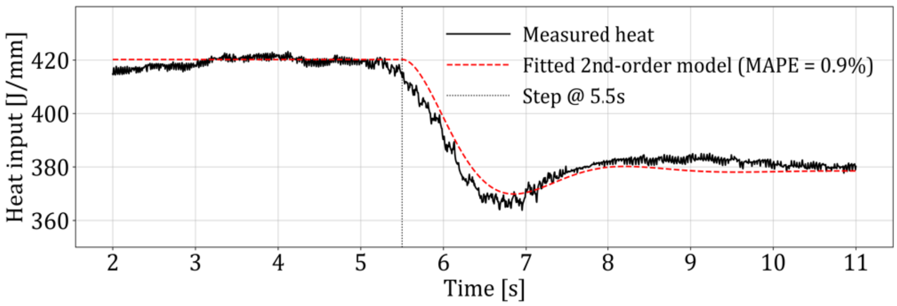

Figure 3. Identified second-order dynamic model and corresponding Laplace-domain transfer function for Invar 36 deposition under the following process conditions: Wire feed speed of 6 m/min, welding speed of 7.5 mm/s, argon shielding gas flow rate of 12.5 L/min, and welding voltage of 20 V

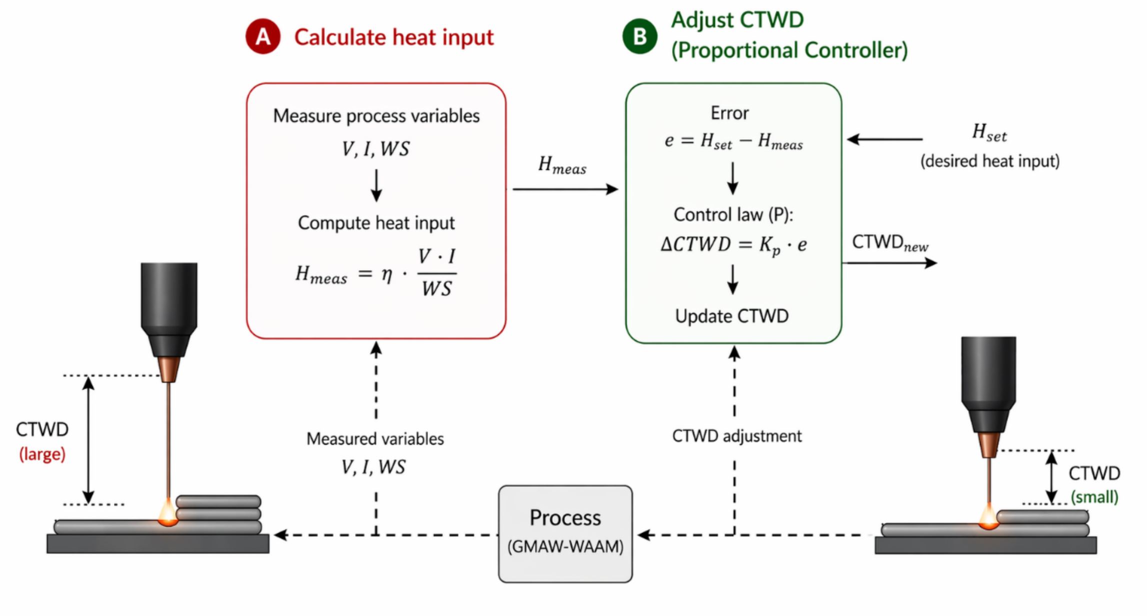

Figure 4. Representative data flow architecture of the proposed controller

welding time. In addition, the geometry of each deposited layer was measured, and the deposited mass was estimated by assuming a rectangular cross-sectional profile, using **Equation 4**, and an Invar density of 8.05×10^3 kg/m^3. The results are reported in Table 2 for Set 1, Table 3 for Set 2, and Table 4 for Set 3.

$$\hat{m} = \rho V = \rho AL = \rho whL \quad with\ L = 75\ mm \tag{4}$$

It should be noted that this approach represents a geometrical simplification, since WAAM beads generally exhibit rounded and locally irregular cross-sections rather than perfectly rectangular profiles. Therefore, the layer-wise mass values reported below should be interpreted as equivalent estimates used mainly for comparison between open-loop and closed-loop conditions, which may introduce uncertainty in the absolute mass values.

After deposition, all specimens were sectioned to evaluate their internal quality, with particular attention to the absence of voids and porosity. The results showed that all specimens, irrespective of whether they were produced under open-loop or closed-loop conditions, exhibited high internal quality and no detectable defects, as shown in Figure 5. This suggests that both manufacturing strategies are suitable for reliable and high-quality production. Therefore, the assessment of the potential benefits of the closed-loop strategy over the open-loop approach should be primarily based on the following analyses, particularly those related to the efficiency and sustainability outcomes, rather than only on internal quality differences.

Table 2. Data collected for Set 1

Condition	Layer	Width (mm)	Height (mm)	Mass (g)	Mean power (W)
Open loop with 340 J/mm	1	6.4	2.3	8.9	2620.8
	2	6.6	2.1	8.3	2557.3
	3	6.9	2.4	9.9	2528.5
	4	7.2	1.7	7.4	2556.7
	5	6.9	2.1	8.5	2487.3
	6	6.6	2.2	8.7	2499.7
	7	6.7	2.0	8.1	2521.6
	8	7.2	2.0	8.7	2477.4
	9	7.0	2.2	9.3	2470.1
	10	6.6	2.0	7.9	2605.0
	11	7.2	1.7	7.4	2489.8
	12	7.1	2.2	9.4	2722.9
	13	6.2	1.3	4.8	2628.9
	14	6.6	2.2	8.8	2383.4
	15	6.4	2.3	8.9	2454.4
	16	6.2	1.8	6.7	2443.9
	17	6.6	1.9	7.5	2394.3
	18	6.2	2.5	9.3	2479.5
	19	6.7	1.8	7.3	2493.4
	20	7.0	1.8	7.5	2620.8
Closed loop with 340 J/mm	1	7.8	1.9	8.9	2579.1
	2	7.9	2.0	9.5	2617.0
	3	8.7	2.1	11.0	2662.6
	4	7.9	2.1	10.1	2657.8
	5	8.1	2.1	10.3	2589.3
	6	8.5	2.1	10.8	2590.1
	7	8.3	2.1	10.6	2692.4
	8	8.7	1.8	9.4	2668.4
	9	8.2	2.1	10.4	2586.7
	10	8.2	2.1	10.4	2582.4
	11	8.4	1.9	9.7	2702.3
	12	8.6	2.0	10.4	2701.1
	13	8.3	2.1	10.6	2599.3
	14	8.2	2.1	10.4	2619.5
	15	8.3	1.6	8.0	2674.1
	16	8.5	2.1	10.8	2879.3
	17	8.4	2.1	10.7	2628.1
	18	8.4	1.9	9.7	2591.9
	19	8.3	1.9	9.5	2576.6
	20	8.3	2.1	10.6	2627.9

Note: Reference condition = 340 J/mm.

Table 3. Data collected for Set 2

Condition	Layer	Width (mm)	Height (mm)	Mass (g)	Mean power (W)
Open loop with 380 J/mm	1	7.1	2.0	8.7	2816.6
	2	7.3	2.3	10.2	2797.6
	3	7.6	1.2	5.5	2752.1
	4	7.3	2.0	8.8	2828.0
	5	7.9	1.4	6.6	2878.2
	6	7.7	2.3	10.7	2897.8
	7	8.0	1.8	8.7	2923.5
	8	7.6	1.9	8.7	2883.4
	9	7.7	1.6	7.5	2895.3
	10	7.3	2.0	8.8	2849.1
	11	7.5	1.7	7.7	2816.4
	12	7.5	2.1	9.5	2835.2
	13	7.9	2.0	9.5	2777.6
	14	7.5	1.8	8.1	2863.3
	15	8.0	2.0	9.7	3004.2
	16	7.4	1.8	8.0	2863.3
	17	7.6	1.5	6.9	2767.7
	18	7.6	2.0	9.2	2771.0
	19	7.5	1.5	6.7	2752.7
	20	7.6	1.7	7.8	2681.6
Closed loop with 380 J/mm	1	8.4	1.9	9.7	2876.3
	2	9.0	1.8	9.8	2896.3
	3	9.0	2.0	10.8	2873.6
	4	9.0	2.3	12.5	2887.4
	5	9.0	2.2	12.0	2878.0
	6	8.9	2.1	11.3	2856.8
	7	9.0	2.3	12.5	2957.6
	8	9.0	1.8	9.8	2873.6
	9	9.0	2.0	10.8	2895.8
	10	9.0	2.1	11.3	2891.5
	11	8.9	1.9	10.2	2847.3
	12	9.0	2.2	12.0	2877.6
	13	9.0	2.1	11.3	2890.2
	14	8.9	2.1	11.3	2900.0
	15	8.9	2.1	11.3	2806.8
	16	8.9	2.1	11.2	2851.2
	17	8.8	2.1	11.1	2859.5
	18	8.9	1.9	10.2	2959.1
	19	8.9	1.9	10.2	2859.7
	20	8.9	2.2	11.8	2848.1

Note: Reference condition = 380 J/mm.

Table 4. Data collected for Set 3

Condition	Layer	Width (mm)	Height (mm)	Mass (g)	Mean power (W)
Open loop with 400 J/mm	1	8.0	2.0	9.7	2976.1
	2	7.7	2.1	9.8	2960.5
	3	8.1	1.9	9.3	3176.4
	4	8.2	1.4	6.9	2882.2
	5	8.1	2.0	9.8	2866.8
	6	8.0	2.0	9.7	2871.3
	7	8.8	2.4	12.7	2903.0
	8	7.8	1.5	7.1	2954.1
	9	8.2	1.5	7.4	2839.5
	10	8.3	1.9	9.5	2832.2
	11	8.0	2.0	9.5	2849.3
	12	7.7	2.2	10.2	2767.7
	13	7.5	2.2	9.9	2842.6
	14	7.6	1.3	6.0	2717.1
	15	7.6	2.1	9.7	2928.8
	16	7.6	1.4	6.4	2610.7
	17	7.7	2.2	10.2	2826.3
	18	7.5	1.6	7.1	2673.2
	19	7.2	1.6	6.9	2587.8
	20	7.2	1.4	6.1	2976.1
Closed loop with 400 J/mm	1	9.9	2.1	12.5	3014.7
	2	9.7	2.0	11.7	3073.1
	3	9.7	2.1	12.2	3009.7
	4	9.6	1.8	10.4	2993.3
	5	9.9	1.9	11.3	2987.7
	6	10.0	2.0	12.1	3039.5
	7	10.0	1.9	11.5	2973.3
	8	10.1	1.7	10.3	2977.8
	9	9.8	2.0	11.8	2950.2
	10	10.1	1.7	10.3	2918.5
	11	9.8	2.0	11.8	3035.5
	12	9.8	1.6	9.4	2919.3
	13	9.8	1.6	9.4	2894.8
	14	9.9	1.9	11.3	2801.4
	15	9.7	1.6	9.4	2797.9
	16	9.7	1.6	9.4	2817.0
	17	9.7	1.7	9.9	2878.8
	18	9.9	1.7	10.2	2992.9
	19	9.8	1.7	10.1	2932.3
	20	9.7	1.8	10.6	2815.1

Note: Reference condition = 400 J/mm.

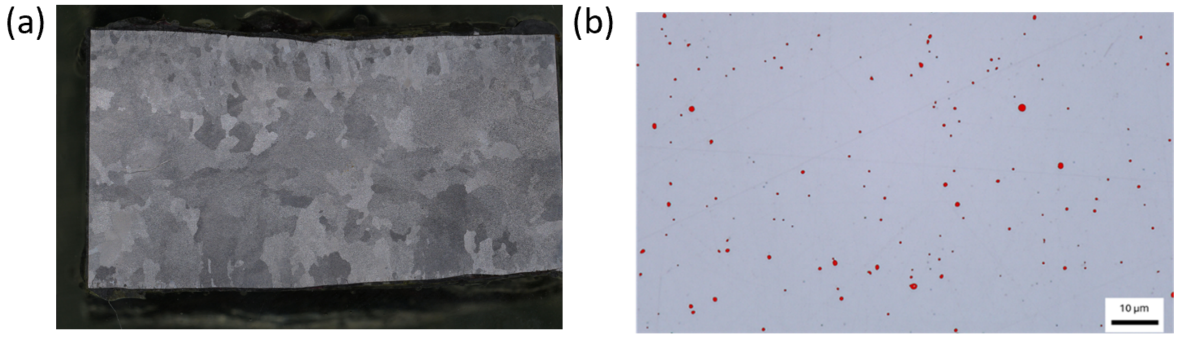

Figure 5. Representative inspection of the deposited Invar 36 wall: (a) Macrograph of a transverse section; (b) micro-scale inspection showing limited dispersed porosity

2.4. Life cycle assessment methodology

Life cycle assessment (LCA) is a standardised methodology, according to ISO 14040 and ISO 14044, for evaluating the environmental aspects and potential impacts of a product or process over its life cycle.[33] The framework is structured into four phases: goal and scope definition; life cycle inventory (LCI), where all relevant inputs, including materials, energy, and consumables, and outputs, such as emissions and waste, are quantified for each process within the system; life cycle impact assessment (LCIA), in which inventory flows are translated into environmental impact indicators through characterisation methods; and interpretation, in which the results are critically analysed with respect to the objectives of the study. In this work, the LCI was developed on the basis of the experimental campaign and the datasets obtained during process monitoring described in the previous section.

A layer-by-layer LCA was carried out to quantify the environmental implications of the WAAM process under both open-loop and closed-loop operating conditions. The model was developed in SimaPro 9.6 by combining measured data from the experimental campaign with the selected background datasets, namely EcoInvent V3. Environmental impacts were assessed using the European CML-IA baseline v3.10 midpoint method.

In particular, the WAAM process inventory included three main contributions: electrical energy consumption, argon shielding gas consumption, and process-related arc welding emissions. Electricity consumption was modelled using the medium-voltage electricity transformation dataset available in EcoInvent. Argon consumption was modelled using the 'market for argon, crude, liquid' dataset. The Invar 36 wire production was modelled separately, starting from its main constituent materials, nickel and low-alloy steel, combined with hot rolling and wire drawing processes. In addition, the welding arc process dataset was included to account for process-related emissions associated with arc deposition.

While a preliminary screening included additional midpoint categories, namely acidification potential (AP), eutrophication potential (EP), and ozone depletion potential (ODP), the analysis presented in this work focuses exclusively on GWP over a 100-year time horizon (GWP100), expressed in $kgCO_2$-eq. The system boundaries were defined according to a cradle-to-gate perspective and were restricted to the manufacturing stage of the deposited material. The life cycle inventory was developed on a layer-by-layer basis and included the consumption of filler material, electrical energy, shielding gas, and process-related emissions.

For each layer, the deposited mass was first estimated from the corresponding layer geometry and the material density, as described above. All inventory flows were then normalised with respect to the deposited mass, in order to express the environmental burdens per kilogram of deposited material. The electrical energy demand was calculated from the process signals acquired during deposition. In particular, the instantaneous power was obtained from the measured voltage and current:

$$P_l(t) = V_l(t) I_l(t), \tag{5}$$

and the layer-wise electrical energy consumption was estimated as:

$$E_l = \int_{t_{0,l}}^{t_{1,l}} P_l(t)\, dt. \tag{6}$$

The specific energy consumption was then calculated by scaling the layer energy demand by the deposited mass:

$$SEC_l = \frac{E_l}{m_l} \tag{7}$$

where SEC_l is expressed in $\frac{kWh}{kg}$. The same massnormalisation procedure was applied to the other inventory flows, including filler material, shielding gas, and process-related emissions. The modelling procedure is illustrated in Figure 6, which reports an example of one of the modelled layers. The shielding gas contribution was also included in the inventory. Although the argon flow rate was kept constant (12.5 L/min) for all experiments, and therefore did not contribute significantly to the variability observed between layers, it still represented a non-negligible contribution to the total GWP and was therefore retained in the assessment. Consequently, the variability of the layer-wise GWP was mainly driven by fluctuations in mass deposition rate and specific energy consumption.

The layer-by-layer LCA was used for two purposes. First, it allowed the environmental behaviour of the process to be analysed along the build direction, highlighting how GWP changed from layer to layer as a consequence of variations in deposition stability and energy efficiency. Second, the average values obtained from the wall specimens were used to derive expected environmental indicators that could subsequently be scaled up from simple geometries to the complex component. In this way, the specimen-level analysis provided both a detailed interpretation of process variability and a predictive basis for estimating the environmental performance of the final part. The full methodology is shown in Figure 7.

2.5. Scale up to industrial application

After deposition of the simple wall geometries and analysis of the control effects on these simplified structures, a more complex geometry representative of a real manufacturing component was produced, as shown in Figure 8. For this component, a heat input reference of 380 J/mm was adopted, while the interpass temperature was maintained at 100 °C, consistent with the conditions previously used for the wall structures. This choice was based on previous experimental observations on Invar 36, which indicated that such conditions allow stable deposition while avoiding excessive substrate heating, a factor that may promote local collapse of the upper layers due to the specific thermo-mechanical behaviour of the alloy.[34]

This enabled comparison between the results obtained on simple geometries and those measured on a real part, in order to evaluate how reliably the former can approximate the behaviour of an actual component. During deposition, energy consumption was monitored continuously, while the final mass of the components manufactured under open-loop and closed-loop conditions was measured.

3. Results and discussion

Tables 1–3 report the layer-wise experimental data collected for the three investigated reference heat input conditions, namely 340, 380, and 400 J/mm, under both open-loop and closed-loop operation. For each deposited layer, the measured quantities include bead width, bead height, deposited mass, and mean electrical power. These quantities represent the direct experimental outputs used as the basis for the subsequent comparative analysis of process productivity and energy performance. To enable a consistent comparison between open-loop and closed-

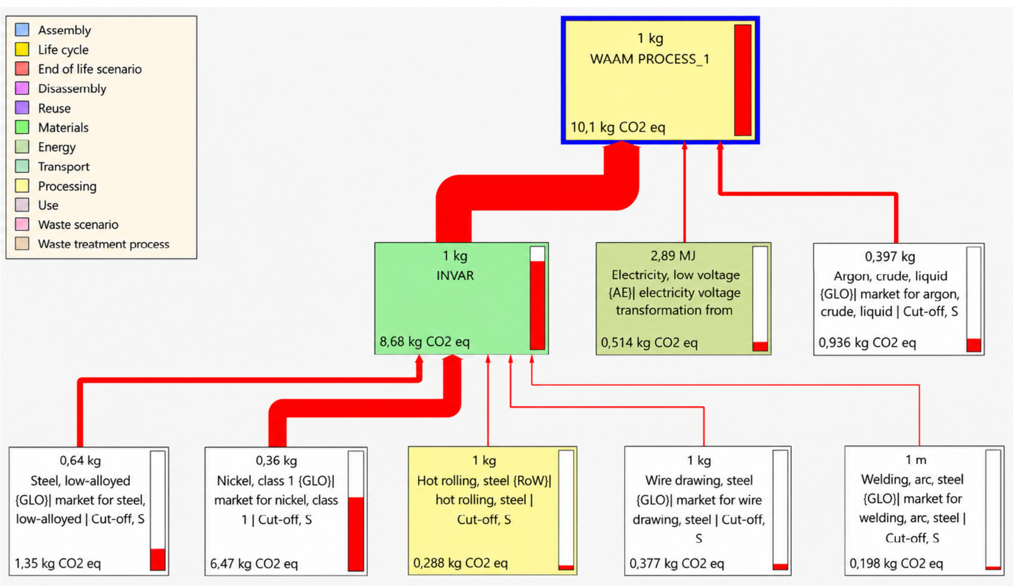

Figure 6. Example of the SimaPro model developed to estimate the global warming potential (GWP) based on life cycle inventory (LCI) data

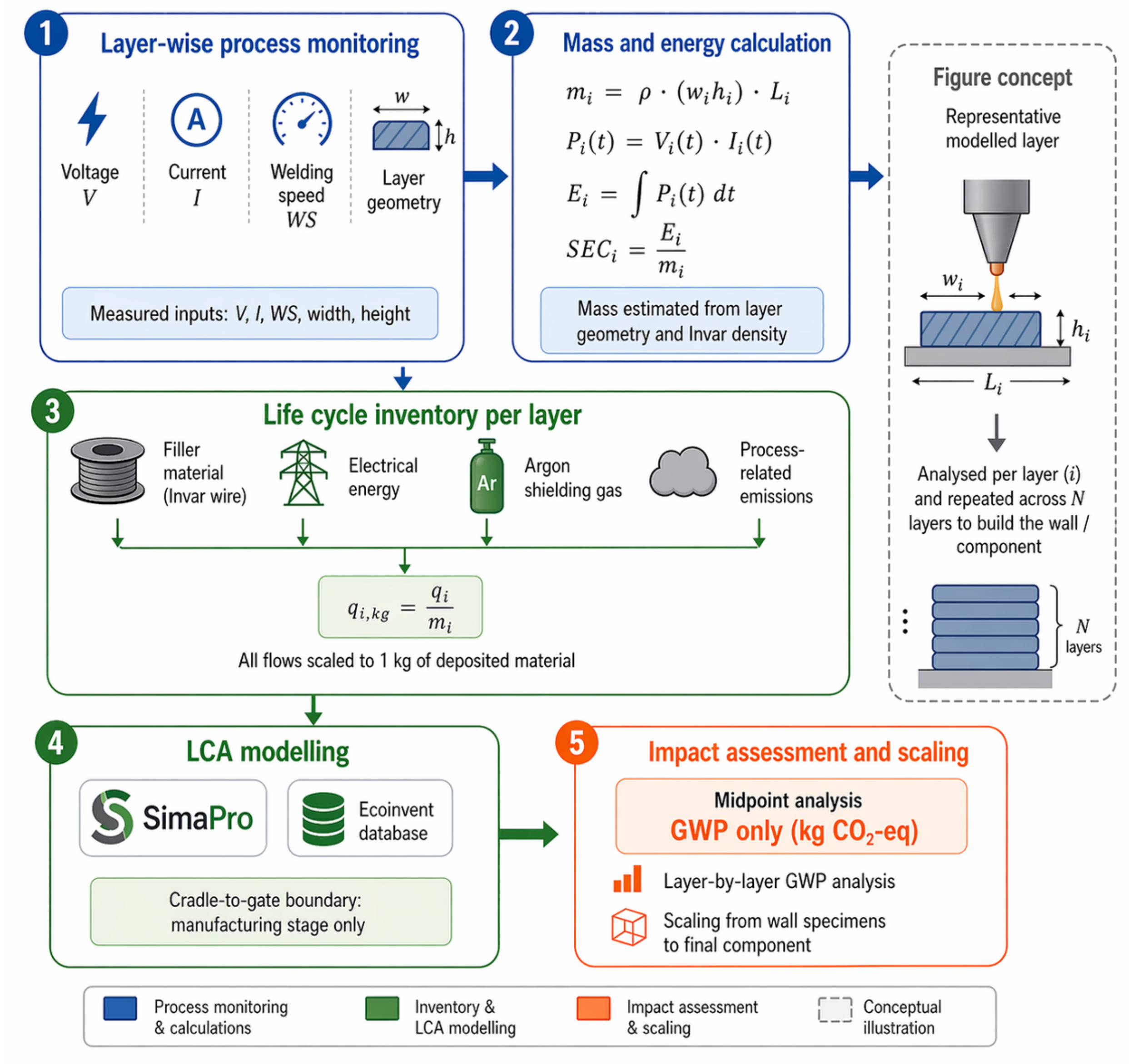

Figure 7. Life cycle assessment (LCA) methodology for layer-wise environmental assessment

loop conditions, the raw layer-wise measurements were further processed into two derived indicators. First, the deposited mass was normalised by the deposition time (t_w) of each layer, to obtain the mass deposition rate:

$$\dot{m} = \frac{m_{\text{layer}}}{t_w}\left[\frac{\text{kg}}{\text{s}}\right] \tag{8}$$

Second, the mean electrical power recorded for each layer was converted into energy per layer and then normalised by the deposited mass, thus obtaining the specific energy consumption:

$$SEC = \frac{P_{\text{mean}} \cdot t_w}{3.6 \times 10^6 \cdot m_{\text{layer}}}\left[\frac{\text{kWh}}{\text{kg}}\right] \tag{9}$$

where P_{mean} is the mean power measured during deposition of the considered layer, and 3.6×10^6 is the conversion factor from J to kWh. The normalised indicators were introduced to support a more meaningful comparison of the two control strategies: the mass deposition rate reflects process productivity, while the specific energy consumption quantifies the electrical energy required per unit mass of deposited material.

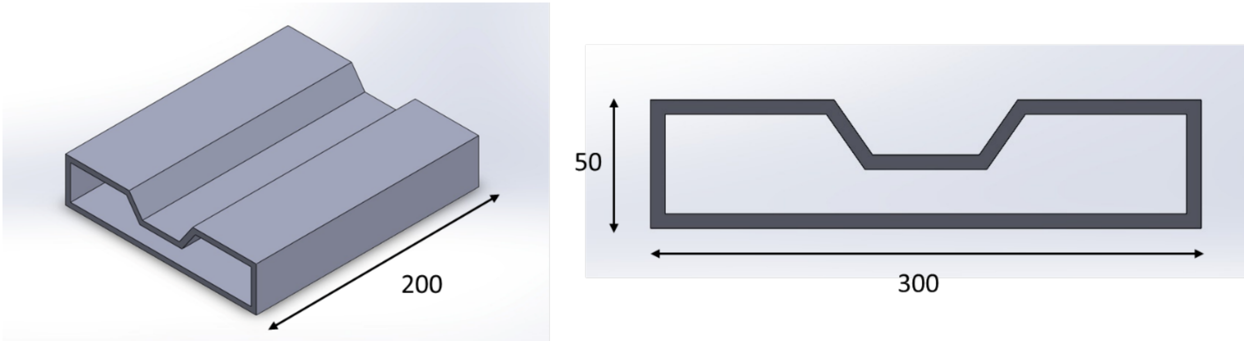

Figure 8. Complex WAAM geometry representative of a real manufacturing component, used to compare predicted and measured energy consumption under open-loop and closed-loop conditions of Invar 36 alloy

3.1. Impact on mass consumption

Analysis of the mass-related results shows that the introduction of the feedback control loop had a clear effect on the mass deposited per layer across all the investigated heat input references. Compared with the open-loop condition, the closed-loop strategy systematically yielded higher and more stable layer mass values, suggesting more regular material transfer and more consistent deposition behaviour throughout the build. By maintaining the heat input within a defined range, the control action promotes more stable bead formation and, consequently, greater uniformity in the resulting layer geometry.

As shown in Figure 9, for the 340 J/mm condition, the average deposited mass increased from 8.230 to 10.145 g per layer, corresponding to a rise in mass deposition rate from 0.8230 to 1.0145 g/s (+23.3%). At the same time, the coefficient of variation of mass along the layers decreased from 14.51% to 8.41%, which indicates a marked improvement in layer-to-layer regularity.

A similar, and even stronger, trend was observed for the 380 J/mm condition, shown in Figure 10. The mean layer mass increased from 8.265 to 11.055 g, corresponding to an increase in mass deposition rate from 0.8265 to 1.1055 g/s (+33.8%). In parallel, the variability of mass deposition was nearly halved, with the coefficient of variation decreasing from 15.95% to 7.81%. Finally, at 400 J/mm, as shown in Figure 11, the same overall behaviour was observed. The average mass increased from 8.805 to 10.780 g per layer, corresponding to a deposition-rate increase from 0.8805 to 1.0780 g/s (+22.4%). More importantly, the coefficient of variation dropped from 20.36% in open loop to 9.64% in closed loop, confirming that feedback control effectively damped the process fluctuations that became more evident at the highest tested reference.

In practical WAAM terms, this means that the closed-loop strategy improved deposition continuity and reduced the occurrence of locally thin layers, which is essential for preserving wall integrity and geometric repeatability.

3.2. Impact on energy consumption

The analysis of energy consumption shows that the feedback control loop did not reduce the average electrical power input in absolute terms. On the contrary, a slight increase in mean power was observed in all three datasets. For the 340 J/mm condition, as illustrated in Figure 12, the mean power increased from 2521.8 W in open loop to 2641.3 W in closed loop (+4.7%). Despite this, the specific energy consumption decreased from 0.874 to 0.728 kWh/kg (−16.7%). This result indicates that the additional power demanded by the controller was more than compensated for by the higher deposited mass, yielding a more energy-efficient deposition process on a per-mass basis. The closed-loop condition also reduced the variability of specific energy, with the coefficient of variation decreasing from 20.29% to 9.06%, which further confirms a more regular thermo-electrical process state.

The 380 J/mm condition, as shown in Figure 13, provided the most favourable result in terms of energy efficiency. The mean power changed only marginally, from 2832.7 to 2879.3 W (+1.6%), whereas the specific energy consumption dropped from 0.975 to 0.728 kWh/kg (−25.4%). At the same time, the variability of specific energy was reduced from 16.27% to 7.95%. This combination of nearly unchanged mean power, substantially increased deposited mass, and improved stability suggests that the 380 J/mm reference offered the best compromise between process intensity and deposition efficiency under feedback control.

Finally, at 400 J/mm, as shown in Figure 14, the average power increased from 2852.1 to 2941.1 W (+3.1%), while the specific energy consumption decreased from 0.935 to 0.763 kWh/kg (−18.3%). Moreover, the closed-loop condition exhibited a marked reduction in specific-energy variability, with the coefficient of variation falling from 20.23% to 8.15%.

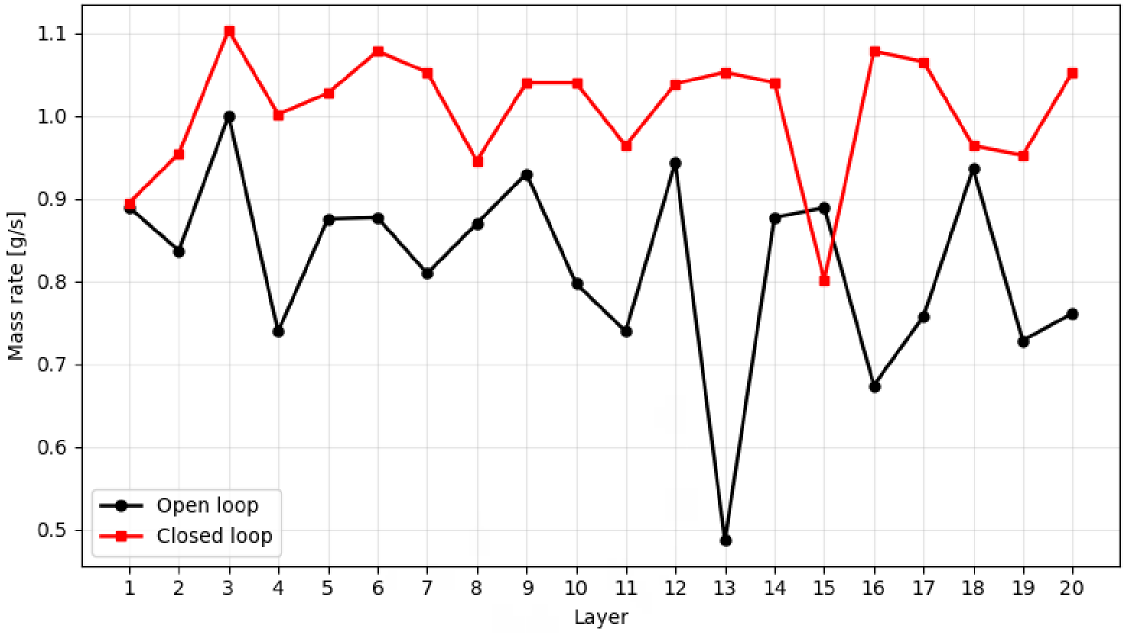

Figure 9. Mass rate per layer behaviour for Set 1 – 340 J/mm

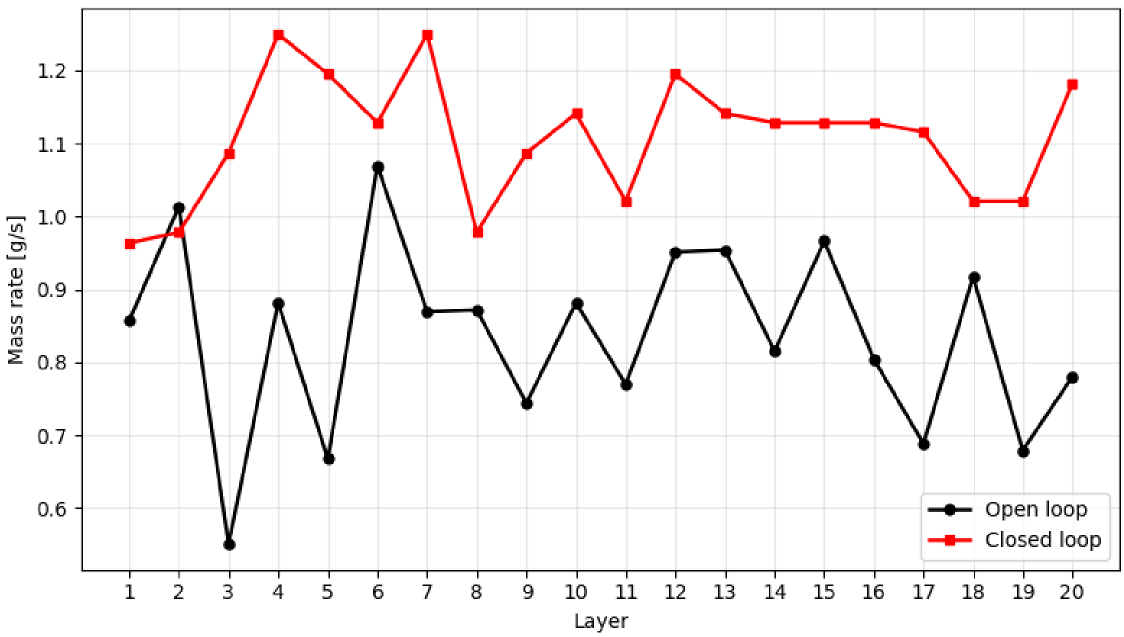

Figure 10. Mass rate per layer behaviour for Set 2 – 380 J/mm

Overall, the results indicate that the proposed feedback control strategy led to a more efficient conversion of electrical energy into deposited material. In other words, although the mass deposition rate increased, the controller also improved the specific energy performance. From the WAAM perspective, this represents a meaningful result, since lower kWh/kg values correspond to a lower electricity-related impact per unit mass of deposited material, provided that the deposited material is effectively utilised in the final component. However, a more detailed and quantitative assessment of the carbon footprint associated with the production stage requires the LCA analysis presented in the following section.

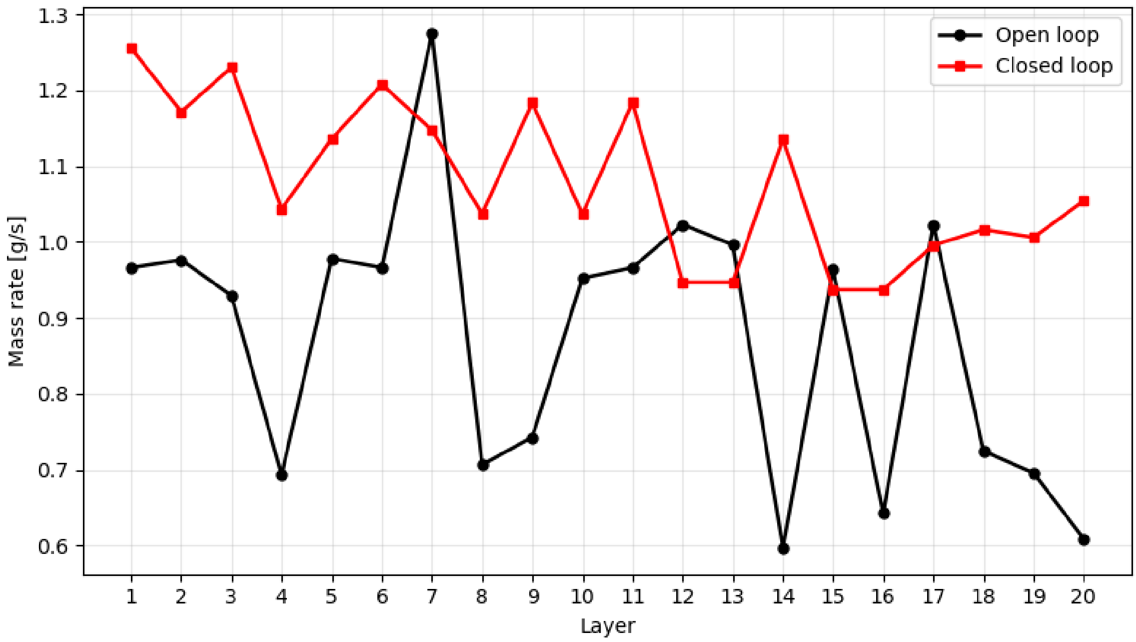

Figure 11. Mass rate per layer behaviour for Set 3 – 400 J/mm

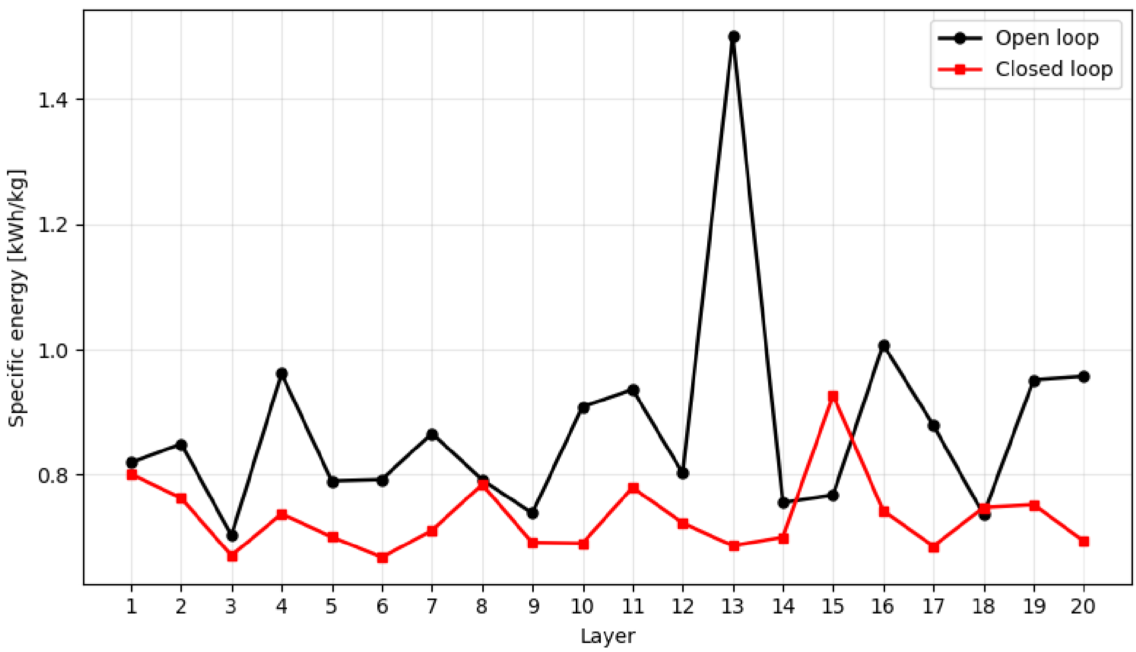

Figure 12. Specific energy per layer behaviour for Set 1 – 340 J/mm

3.3. Impact on carbon footprint

The analysis of the GWP shows that the closed-loop strategy reduced the environmental impact across all the investigated heat input references. This result is consistent with the specific energy analysis reported in the previous section. Although the closed-loop condition did not reduce the average electrical power demand in absolute terms, it increased the deposited mass and improved the stability of the deposition process. As a result, the environmental impact expressed in terms of GWP decreased in all cases. In accordance with previous work, the production of Invar feedstock was assumed to contribute 8.68 kg CO_2-eq per kg of deposited material. As the results were normalised on a mass basis, this contribution was not included in the

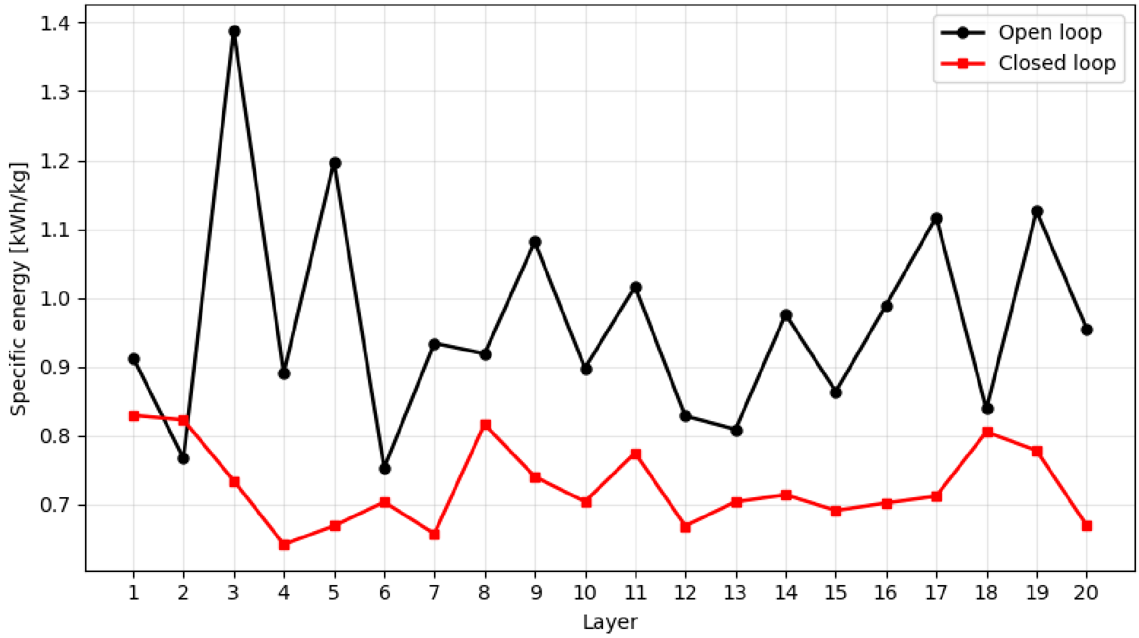

Figure 13. Specific energy per layer behaviour for Set 2 – 380 J/mm

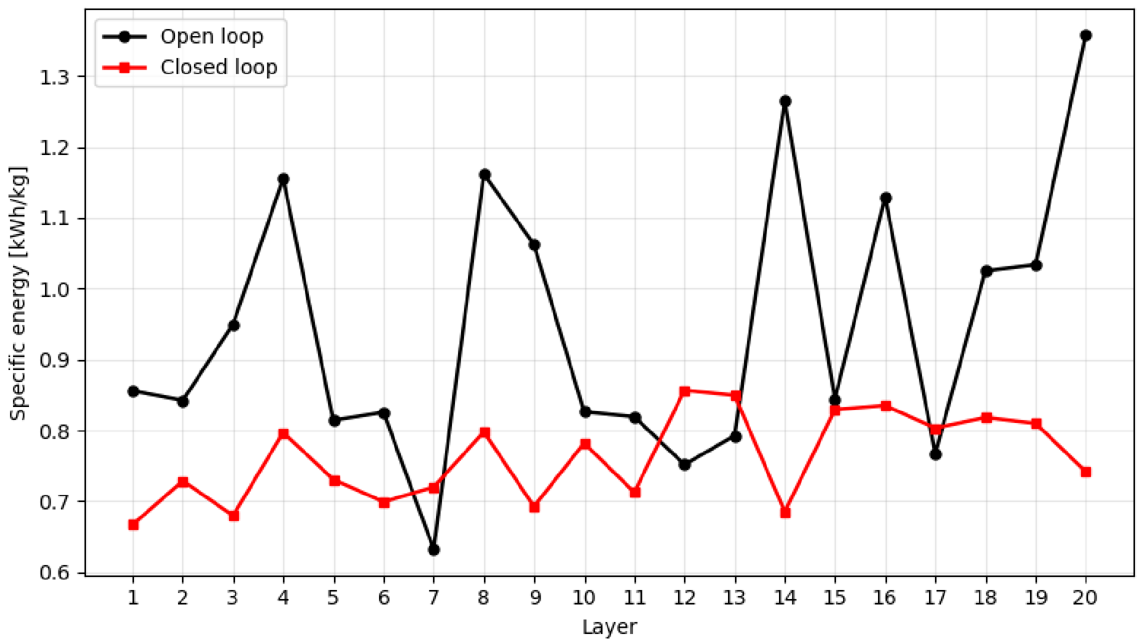

Figure 14. Specific energy per layer behaviour for Set 3 – 400 J/mm

comparative assessment, since it represents a constant material-related offset across the analysed conditions. The analysis was therefore focused on the WAAM contributions associated with electricity consumption, argon use, and layer-by-layer process emissions, which are more directly influenced by the deposition parameters and control strategy. Therefore, the GWP values discussed in this section refer specifically to the WAAM process contribution (WAAM-only) and should be distinguished from the total component-scale carbon footprint, which also includes the dominant contribution associated with Invar feedstock production.

For the 340 J/mm condition, shown in Figure 15, the mean GWP decreased from 1.594 kg CO_2-eq/kg in open loop to 1.285 kg CO_2-eq/kg in closed loop, corresponding to a reduction of 19.4%. In addition to the reduction in the average value, the variability of the environmental impact was also markedly reduced. The coefficient of variation decreased from 19.99% in open loop to 8.51% in closed loop. This indicates that the feedback control strategy not only lowered the average GWP, but also produced a more stable environmental performance along the deposited layers.

A similar trend was observed for the 380 J/mm condition, as illustrated in Figure 16. In this case, the mean GWP decreased from 1.652 kg CO_2-eq/kg in open loop to 1.229 kg CO_2-eq/kg in closed loop, corresponding to a reduction of 25.6%. This was the largest reduction among the investigated conditions. The coefficient of variation also decreased from 16.76% to 8.73%, confirming the improved regularity of the process under closed-loop control. This result is particularly relevant because the 380 J/mm condition also showed the strongest decrease in specific energy consumption, suggesting that this heat input reference provided the most favourable balance between deposition efficiency and environmental performance.

For the 400 J/mm condition, as shown in Figure 17, the mean GWP decreased from 1.541 kg CO_2-eq/kg in open loop to 1.263 kg CO_2-eq/kg in closed loop, corresponding to a reduction of 18.1%. The reduction in variability was also substantial, with the coefficient of variation decreasing from 21.53% to 8.65%. This confirms that the closed-loop strategy was especially effective in stabilising the environmental response at the highest heat input reference, where the open-loop condition exhibited the largest fluctuations.

Overall, the GWP results confirm the sustainability benefit of the feedback control strategy. The reduction in environmental impact was not caused by a lower average power demand, since the mean power slightly increased under closed-loop conditions. Instead, the improvement was mainly associated with the higher deposited mass, the lower specific energy consumption, and the more stable layer-by-layer deposition behaviour. Therefore, the closed-loop approach enabled a more efficient use of electrical energy and reduced the GWP associated with the production stage. Among the investigated conditions, the 380 J/mm reference provided the best overall outcome, with the largest GWP reduction and the lowest mean specific energy consumption.

3.4. Discussion of the results on wall specimens

The results obtained on the wall specimens show that the closed-loop strategy improved the overall process performance across all the investigated heat input references. Although the feedback control loop led to a slight increase in mean electrical power, this increase

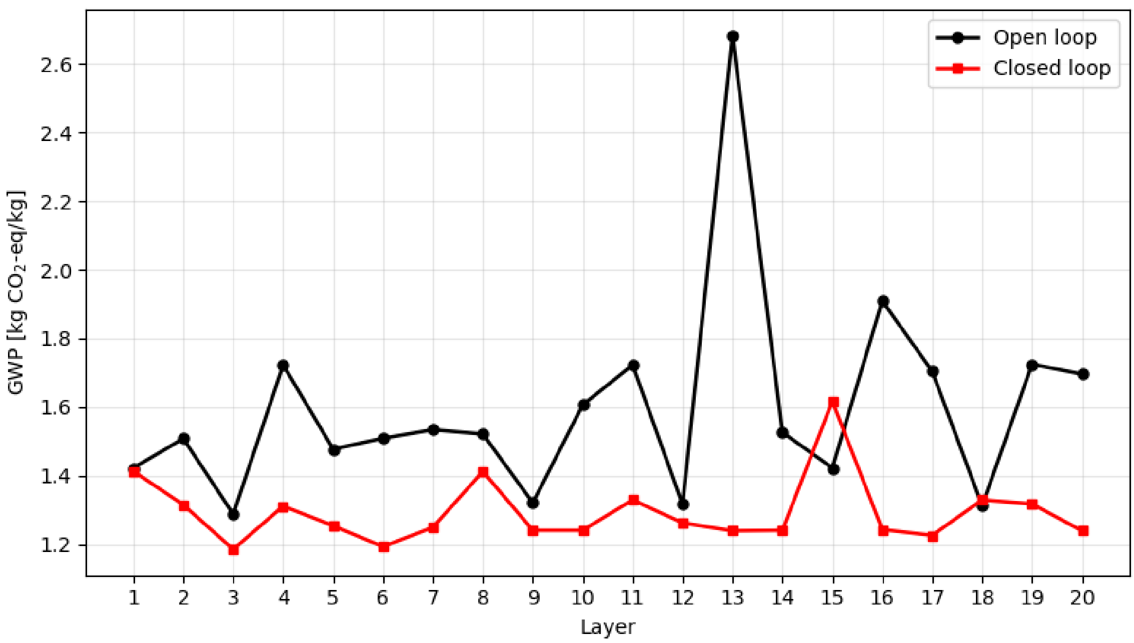

Figure 15. Global warming potential (WAAM-only) per layer behaviour for Set 1 – 340 J/mm

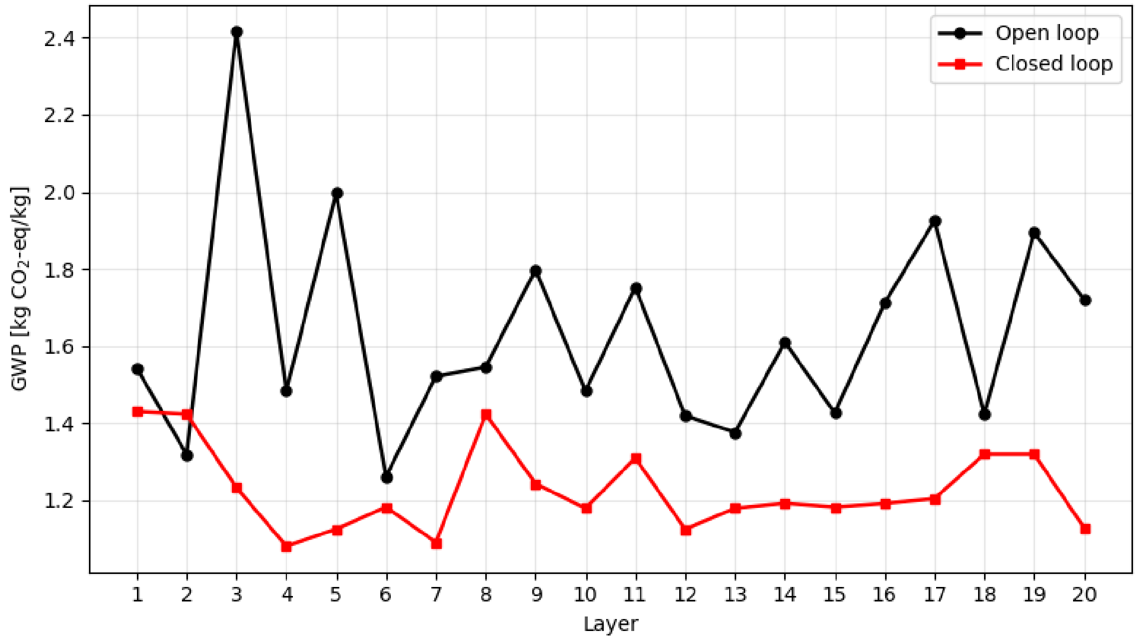

Figure 16. Global warming potential (WAAM-only) per layer behaviour for Set 2 – 380 J/mm

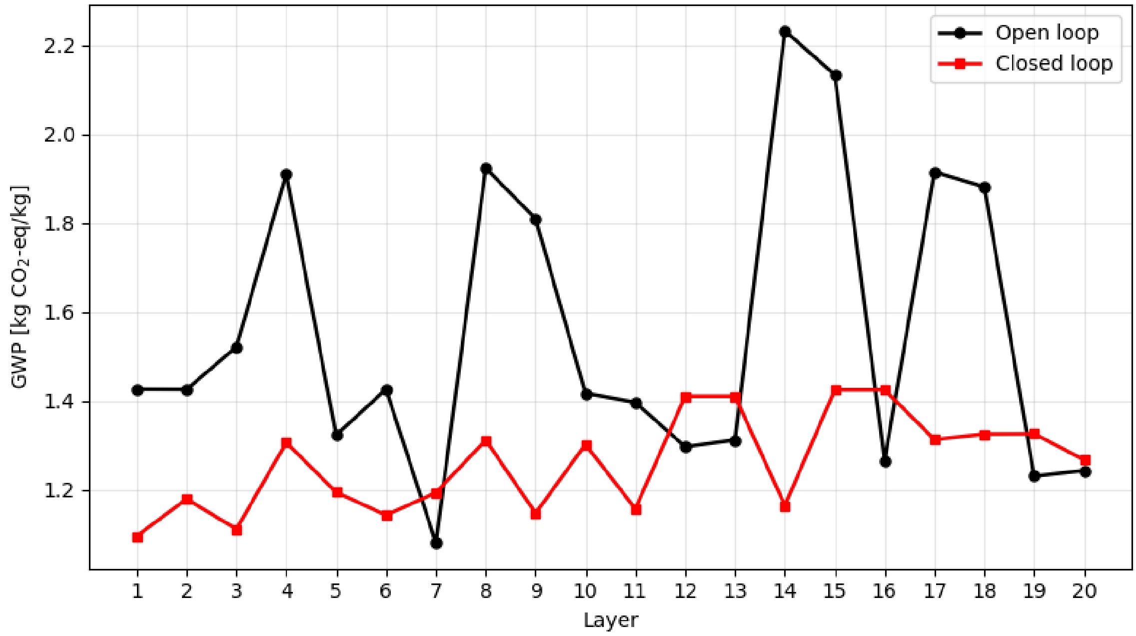

Figure 17. Global warming potential per layer behaviour for Set 3 – 400 J/mm

was compensated for by a higher deposited mass and by a more stable layer-by-layer deposition behaviour. As a consequence, the closed-loop condition consistently reduced both the specific energy consumption and the associated GWP (WAAM-only). Table 5 reports the corresponding values, the percentage reductions achieved by the closed-loop strategy, and the related variations. These results suggest that the main benefit of the feedback control strategy is not associated with a direct reduction in power demand, but rather with a more efficient conversion of electrical energy into deposited material.

Among the tested conditions, 380 J/mm provided the best overall performance, combining the largest increase in mass deposition rate with the greatest reductions in specific energy consumption and GWP. This suggests that, at wall scale, closed-loop control is most effective at an intermediate heat input, where material deposition is enhanced without a substantial increase in power demand. However, since wall specimens represent a simplified and regular deposition case, the next step is to verify whether these benefits are preserved when scaling to a real component, where geometrical complexity, path changes, thermal accumulation and local instabilities may alter the energy and environmental response.

3.5. From simple to complex large-sized geometry

3.5.1. Production time and component weight

Following validation on the thin-wall geometries, the proposed control strategy was applied to the fabrication of a more complex Invar 36 component representative of a real tooling application, adopting a target heat input of 380 J/mm. The final components are shown in Figure 18. During the deposition process, manufacturing time and electrical power were continuously monitored, while the final mass of the components produced under open-loop and closed-loop conditions was measured at the end of the build. The results showed that the component manufactured under closed-loop control reached a final mass of approximately 11 kg, compared with approximately 10 kg for the open-loop condition. This confirms that the proposed controller promotes a higher effective deposition rate also on the real component, in agreement with the trends previously observed on the thin-wall structures. Overall, the controlled strategy enabled a greater amount of material to be deposited within a shorter production time, while preserving the target functional geometry required for the tool.

This aspect is particularly relevant for the present application, as the component was designed as a tool for producing omega stringers in the aerospace composite sector, where the final contour geometry is more critical than strict local thickness control. Therefore, the slightly higher deposited mass obtained under closed-loop operation is not detrimental, provided that the target outside shape is maintained. Moreover, the closed-loop strategy completed the build in 90 layers instead of 100, reducing the total manufacturing time from 3 h 5 min to 2 h 46 min. This higher productivity is further confirmed by the reduction in arc-on time from 2 h 50 min to 2 h 33 min.

3.5.2. Effective mass rate and comparison with the expected outcome from wall specimens

To assess whether the trends identified at the specimen scale were maintained at the component scale, the average mass deposition rates obtained for the 380 J/mm condition were combined with the measured arc-on times of the complex build. For the open-loop condition, an average deposition rate of 0.8805 g/s and an arc-on time of 10,200 s yielded a predicted deposited mass of 8.98 kg, compared

Table 5. Summary of the main results obtained for the wall specimens from GWP in kg CO_2-eq/kg (WAAM-only)

Condition	Open-loop mean	Closed-loop mean	Reduction	Open loop CV	Closed-loop CV
340 J/mm	1.594	1.285	−19.4%	19.99%	8.51%
380 J/mm	1.652	1.229	−25.6%	16.76%	8.73%
400 J/mm	1.541	1.263	−18.1%	21.53%	8.65%

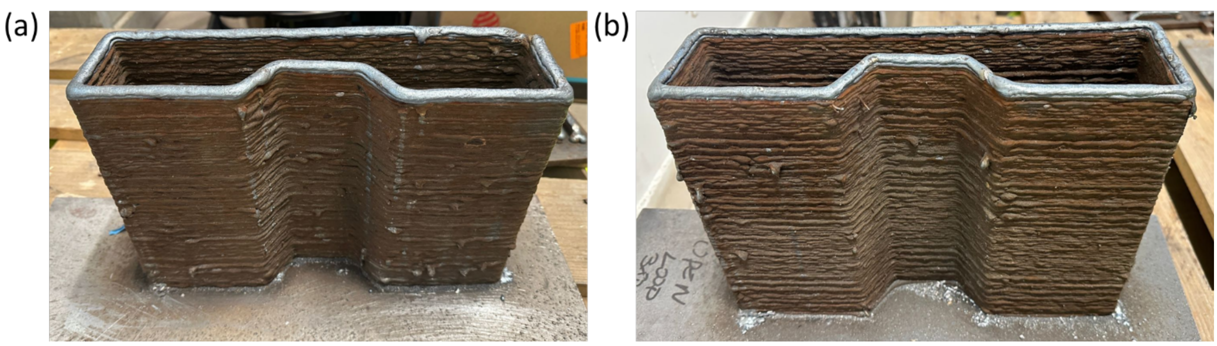

Figure 18. Comparison between the closed-loop (a) and the open-loop fabrication (b) of the complex Invar 36 tooling component

with a measured final mass of 10.0 kg. For the closed-loop condition, using an average deposition rate of 1.101 g/s and an arc-on time of 9,180 s, the predicted deposited mass was 10.10 kg, compared with a measured value of 11.0 kg. These results indicate that the specimen-based approach slightly underestimated the effective productivity of the real component, with mass deviations of approximately 10.2% and 8.2% for the open-loop and closed-loop conditions, respectively.

3.5.3. Effective specific energy consumption and comparison with the expected outcome from wall specimens

The same approach was then applied to estimate the total energy demand of the component. In the open-loop condition, the predicted mass of 8.98 kg combined with the specimen-based specific energy consumption of 0.975 kWh/kg led to an estimated total energy demand of 8.68 kWh, compared with the measured value of 8.17 kWh. In the closed-loop condition, the predicted mass of 10.10 kg and the specimen-based specific energy consumption of 0.728 kWh/kg resulted in an estimated energy demand of 7.35 kWh, compared with the measured value of 7.65 kWh. The open-loop case was slightly overestimated, whereas the closed-loop case was slightly underestimated; however, the average absolute deviation between the estimated and measured energy demand was only approximately 5.1%. This confirms that the wall-specimen results can be effectively transferred to component-scale analysis. In addition, the measured component-scale results confirm the benefit of closed-loop control, reducing the energy required to manufacture the part from 8.17 to 7.65 kWh, corresponding to an energy saving of approximately 6.4%.

3.5.3. Effective carbon footprint and comparison with the expected outcome from wall specimens

To complete the component-scale GWP assessment, the total impact was separated into two contributions: the WAAM process-related contribution and the Invar feedstock production contribution. The former includes electricity consumption, argon use and process-related emissions, whereas the latter was calculated using an Invar production factor of 8.68 kg CO_2-eq/kg.

For the open-loop condition, the specimen-based estimate predicted a deposited mass of 8.98 kg. By combining this value with the specific WAAM process-related GWP obtained from the wall specimens, equal to 1.652 kg CO_2-eq/kg, the estimated WAAM-only contribution was 14.83 kg CO_2-eq. The corresponding feedstock contribution was 77.95 kg CO_2-eq, resulting in a total estimated GWP of 92.78 kg CO_2-eq. When the LCA was repeated using the measured component mass and measured process data, the total GWP was 100.00 kg CO_2-eq, of which 13.20 kg CO_2-eq was associated with the WAAM process only. Therefore, the specimen-based approach underestimated the total GWP by 7.2%, while the WAAM-only contribution was overestimated by 12.4%.

For the closed-loop condition, the specimen-based estimate predicted a deposited mass of 10.10 kg. Using the specific WAAM process-related GWP from the wall specimens, equal to 1.229 kg CO_2-eq/kg, the estimated WAAM-only contribution was 12.41 kg CO_2-eq. The feedstock contribution was 87.67 kg CO_2-eq, leading to a total estimated GWP of 100.08 kg CO_2-eq. The LCA based on the measured component data returned a total GWP of 108.00 kg CO_2-eq, with a WAAM-only contribution of 12.50 kg CO_2-eq. In this case, the total GWP was underestimated by 7.3%, while the WAAM-only contribution was predicted with high accuracy, with an error of only −0.7%. Table 6 reports the comparative analysis between specimen-based predictions and component-scale measurements, including the corresponding estimation errors.

These results show that the specimen-based approach slightly underestimated the total component-scale GWP in both conditions, mainly because of the underestimation of the material-related contribution. However, the WAAM-only contribution was predicted with reasonable accuracy. More importantly, the measured component-scale LCA clearly highlighted the distinction between the WAAM-only contribution and the total component-scale carbon footprint. The closed-loop strategy reduced the process-related environmental impact, with the WAAM-only contribution decreasing from 13.20 to 12.50 kg CO_2-eq, corresponding to a reduction of approximately 5.3%. Nevertheless, the total carbon footprint increased from 100.00 to 108.00 kg CO_2-eq because of the higher deposited mass and the dominant contribution associated with Invar feedstock production.

3.6. Final remarks and future research direction

The results of this study show that, for the same nominal process parameters and heat input reference, the closed-loop strategy enabled a higher amount of material to be deposited compared with the open-loop condition. Since the heat input was actively regulated around the target value, this increase in deposited mass was achieved without a proportional increase in energy demand. As a result, the closed-loop approach improved the process efficiency, reducing the specific energy consumption and the WAAM process-related carbon footprint per unit mass of deposited material.

At the wall-specimen scale, this behaviour was particularly evident. The closed-loop strategy increased

Table 6. Summary of specimen-based predictions and component-scale measurements for the open-loop and closed-loop conditions

Condition	Parameter	Value
Open loop	MDR estimated from the specimen	0.8805 g/s
	MDR estimation error from a specimen of the real component	−10.2%
	SEC from the specimen	0.817 kWh/kg
	SEC estimation error from a specimen of the real component	+6.2%
	GWP from the specimen (WAAM-only)	1.62 kg CO_2-eq/kg
	GWP estimation error from a specimen of the real component	−12.4%
Closed loop	MDR estimated from the specimen	1.101 g/s
	Estimation error from a specimen of the real component	−8.2%
	SEC from the specimen	0.765 kWh/kg
	Estimation error from a specimen of the real component	−3.9%
	GWP from the specimen (WAAM-only)	1.24 kg CO_2-eq/kg
	GWP estimation error from a specimen of the real component	−7.3%

Abbreviations: GWP: Global warming potential; MDR: Mass deposition rate; SEC: Specific energy consumption; WAAM: Wire arc additive manufacturing.

the deposited mass per layer and reduced both the specific energy consumption and the process-related GWP. When the constant contribution associated with Invar wire production was excluded, the results clearly indicated that the feedback controller improved the efficiency of the deposition process itself. In other words, for the same amount of deposited material, the closed-loop condition required less energy and generated a lower process-related environmental impact.

However, the component-scale analysis highlighted an important limitation. In the present study, the control strategy regulated the heat input but did not directly control the final deposited geometry or the total deposited mass. Consequently, the closed-loop condition produced a heavier component. While the estimated WAAM process-related GWP decreased from 14.83 to 12.41 kg CO_2-eq, corresponding to a 16.3% reduction, the feedstock-related contribution increased from 77.95 to 87.67 kg CO_2-eq because of the higher deposited mass. Therefore, once Invar wire production was included, the estimated total component-scale GWP increased from 92.78 to 100.08 kg CO_2-eq. This confirms that the environmental advantage of closed-loop control can be partially offset, or even reversed, if the additional deposited material is not required by the final component geometry.

Therefore, the main outcome of this work is twofold:

(i) First, closed-loop heat input control improves the intrinsic efficiency of the WAAM process by increasing deposition rate and reducing the energy and process-related emissions per unit mass.
(ii) Second, to fully translate these benefits into a lower total carbon footprint at the component scale, the control strategy must also account for the amount of material deposited. In WAAM, where feedstock production represents a dominant contribution to the total environmental impact, process efficiency alone is not sufficient if it leads to unnecessary material over-deposition.

Future research should therefore focus on the integration of heat input control with geometry- or mass-based feedback control. Such an approach would allow the process to maintain the benefits observed in this study, namely higher deposition efficiency, reduced specific energy consumption and lower process-related GWP, while avoiding excessive material deposition. In this perspective, future closed-loop WAAM systems should not only stabilise the thermal and electrical behaviour of the process, but also regulate bead geometry, wall thickness, layer height or deposited mass according to the target component requirements. This would make it possible to exploit the full potential of feedback control for sustainable component-scale manufacturing, reducing both process-related emissions and the total carbon footprint of the final part.

4. Conclusion

This work investigated the environmental implications of feedback-controlled heat input in WAAM of Invar 36 using online CTWD adjustment. The study combined layer-wise process monitoring, thin-wall experiments, LCA modelling and scale-up to a complex tooling component. The main conclusions are as follows:

(i) First, closed-loop heat-input control improved deposition regularity and increased the effective deposited mass across all the investigated heat-input references. Compared with open-loop operation, the deposited mass per layer increased by 23.3%, 33.8% and 22.4% at 340, 380 and 400 J/mm, respectively. This confirms that heat-input regulation through CTWD adjustment can stabilise the deposition process and enhance material transfer without modifying the nominal welding parameters.

(ii) Second, the increase in deposited mass was not accompanied by a proportional increase in energy demand. Although the mean electrical power slightly increased under closed-loop conditions, the specific energy consumption decreased by 16.7%, 25.4% and 18.3% for the 340, 380 and 400 J/mm conditions, respectively.

(iii) Third, the layer-wise LCA confirmed that the closed-loop strategy reduced the WAAM process-related carbon footprint. Excluding the constant contribution associated with Invar feedstock production, the WAAM-only GWP decreased by 19.4%, 25.6% and 18.1% for the 340, 380 and 400 J/mm conditions, respectively. This demonstrates that the environmental benefit of the controller is mainly associated with a more efficient conversion of electrical energy and consumables into deposited material.

(iv) Fourth, the trends observed on thin-wall specimens were confirmed at component scale. For the Invar 36 tooling geometry produced at 380 J/mm, closed-loop control reduced the total measured energy demand from 8.17 to 7.65 kWh, corresponding to an energy saving of approximately 6.4%. The measured WAAM-only GWP also decreased from 13.2 to 12.5 kg CO_2-eq, confirming a reduction of approximately 5.3% in the process-related environmental impact.

(v) Finally, the component-scale analysis highlighted a critical limitation. Since the controller regulated heat input but did not directly control the final deposited mass or geometry, the closed-loop component was heavier than the open-loop one. As a result, once the Invar feedstock production contribution was included, the total measured carbon footprint increased from 100 to 108 kg CO_2-eq. This finding shows that heat-input control alone can improve the intrinsic efficiency of WAAM, but does not automatically guarantee a lower total carbon footprint if it leads to material over-deposition.

Overall, the proposed feedback strategy represents a promising route for improving WAAM process stability, productivity and process-related sustainability. However, future closed-loop WAAM systems should integrate heat-input regulation with layer geometry or mass-based feedback control. This would allow the process to retain the observed gains in deposition efficiency and WAAM-only environmental performance while avoiding unnecessary material consumption, which is essential for reducing the total carbon footprint of industrial-scale components.

Acknowledgments

The authors acknowledge the INVITALIA Project NEMESI for their support to this research work.

Funding

The research was funded by the INVITALIA Project NEMESI.

Conflict of interest

Giulio Mattera serves the Editorial Board of this journal as a youth member, but was not in any way involved in the editorial and peer-review process conducted for this paper, directly or indirectly. The authors declare they have no competing interests

Author contributions

Conceptualization: Elena Manoli, Rosa Abate, Yushuai Che, Luigi Nele, Giulio Mattera, Guido Guizzi
Formal analysis: Elena Manoli, Rosa Abate Giulio Mattera
Investigation: Elena Manoli, Rosa Abate, Yushuai Che, Luigi Nele, Giulio Mattera
Methodology: Elena Manoli, Rosa Abate, Luigi Nele, Giulio Mattera, Guido Guizzi
Writing–original draft: Elena Manoli, Rosa Abate, Yushuai Che, Luigi Nele, Giulio Mattera
Writing–review & editing: Elena Manoli, Rosa Abate, Yushuai Che, Luigi Nele, Giulio Mattera

Ethics approval and consent to participate

Not applicable.

Consent for publication

Not applicable.

Availability of data

Data used in this study will be provided upon reasonable request to the corresponding author.

References

1. Xia C, Pan Z, Polden J, *et al*. A review on wire arc additive manufacturing: Monitoring, control and a framework of automated system. *J Manuf Syst*. 2020;57:31-45.

   doi: 10.1016/j.jmsy.2020.08.008

2. Dinh DM, Le VT, Tran VC, *et al*. An experimental–numerical investigation on thermal cycles and their effects on microstructure and mechanical properties in wire arc additive manufacturing of Inconel 625 superalloy rectangular walls. *Weld World*. Published online March 29, 2026.

   doi: 10.1007/s40194-026-02440-z

3. Gil Plazas AF, Amaya Villabón TA, Ramírez Vargas DA, Rubiano Buitrago JD, Herrera Quintero LK. Influence of interlayer thermal cycling on microstructural evolution in WAAM processed carbon steel. *Weld World*. 2026;70(2):471-489.

   doi: 10.1007/s40194-025-02227-8

4. Wu B, Pan Z, Ding D, Cuiuri D, Li H. Effects of heat accumulation on microstructure and mechanical properties of Ti6Al4V alloy deposited by wire arc additive manufacturing. *Addit Manuf*. 2018;23:151-160.

   doi: 10.1016/j.addma.2018.08.004

5. Wu B, Pan Z, Ding D, *et al*. A review of the wire arc additive manufacturing of metals: properties, defects and quality improvement. *J Manuf Process*. 2018;35:127-139.

   doi: 10.1016/j.jmapro.2018.08.001

6. Mattera G, Chozaki SP, Norrish J. Advances in machine learning for parameters optimisation and in-situ monitoring of wire arc additive manufacturing. *Weld World*. 2025;70(4):1173-1202.

   doi: 10.1007/s40194-025-02200-5

7. Xia C, Pan Z, Zhang S, *et al*. Model predictive control of layer width in wire arc additive manufacturing. *J Manuf Process*. 2020;58:179-186.

   doi: 10.1016/j.jmapro.2020.07.060

8. Xiong J, Zhang Y, Pi Y. Control of deposition height in WAAM using visual inspection of previous and current layers. *J Intell Manuf*. 2021;32(8):2209-2217.

   doi: 10.1007/s10845-020-01634-6

9. Shi M, Xiong J. Controlling torch height and deposition height in robotic wire and arc additive manufacturing on uneven substrate. *Weld World*. 2024;68(4):765-779.

   doi: 10.1007/s40194-023-01633-0

10. Chen D, Chen H, Zhang G, Xiong J. Towards automatic control of process stability for thick-wall parts in arc-directed energy deposition based on arc voltage sensing. *J Manuf Process*. 2025;141:250-262.

    doi: 10.1016/J.JMAPRO.2025.03.008

11. Hölscher LV, Hassel T, Maier HJ. Development and evaluation of a closed-loop z-axis control strategy for wire-and-arc-additive manufacturing using the process signal. *Int J Adv Manuf Technol*. 2023;128(3-4):1725-1739.

    doi: 10.1007/s00170-023-12012-w

12. Caggiano A, Mattera G, Zhang Y, Teti R. Heat input control and deep learning-based indirect measure of process and deposition stability in Wire Arc Additive Manufacturing. *CIRP Ann*. 2026;75.

    doi: 10.1016/j.cirp.2026.04.008

13. Kokare S, Oliveira JP, Godina R. Life cycle assessment of additive manufacturing processes: A review. *J Manuf Syst*. 2023;68:536-559.

    doi: 10.1016/j.jmsy.2023.05.007

14. Kokare S, Oliveira JP, Godina R. A LCA and LCC analysis of pure subtractive manufacturing, wire arc additive manufacturing, and selective laser melting approaches. *J Manuf Process*. 2023;101:67-85.

    doi: 10.1016/j.jmapro.2023.05.102

15. Kokare S, Oliveira JP, Santos TG, Godina R. Environmental and economic assessment of a steel wall fabricated by wire-based directed energy deposition. *Addit Manuf*. 2023;61:103316.

    doi: 10.1016/j.addma.2022.103316

16. Priarone PC, Pagone E, Martina F, Catalano AR, Settineri L. Multi-criteria environmental and economic impact assessment of wire arc additive manufacturing. *CIRP Ann*. 2020;69(1):37-40.

    doi: 10.1016/j.cirp.2020.04.010

17. Reis RC, Kokare S, Oliveira JP, Matias JCO, Godina R. Life cycle assessment of metal products: A comparison between wire arc additive manufacturing and CNC milling. *Adv Ind Manuf Eng*. 2023;6:100117.

    doi: 10.1016/j.aime.2023.100117

18. Abate R, Mattera G, Kokare S, Nele L, Guizzi G. Process Parameter Effects on the Environmental Performance of Wire Arc Additive Manufacturing of Invar 36 Alloy: A Life Cycle Assessment Approach. *Sustainability*. 2026;18(8):4106.

    doi: 10.3390/su18084106

19. Aldalur E, Suárez A, Veiga F. Thermal expansion behaviour of Invar 36 alloy parts fabricated by wire-arc additive manufacturing. *J Mater Res Technol*. 2022;19:3634-3645.

    doi: 10.1016/j.jmrt.2022.06.114

20. Huang G, He G, Gong X, He Y, Liu Y, Huang K. Additive manufacturing of Invar 36 alloy. *J Mater Res Technol*. 2024;30:1241-1268.

    doi: 10.1016/j.jmrt.2024.02.221

21. Gil Del Val A, Cearsolo X, Suarez A, Veiga F, Altuna I, Ortiz M. Machinability characterization in end milling of Invar 36 fabricated by wire arc additive manufacturing. *J Mater Res Technol*. 2023;23:300-315.

    doi: 10.1016/J.JMRT.2022.12.182

22. Khanna N, Gandhi A, Nakum B, Srivastava A. Optimization and analysis of surface roughness for INVAR-36 in end milling operations. *Mater Today Proc*. 2018;5(2):5281-5288.

    doi: 10.1016/j.matpr.2017.12.111

23. Sood A, Schimmel J, Ferreira VM, *et al*. Directed energy deposition of Invar 36 alloy using cold wire pulsed gas tungsten arc welding: Effect of heat input on the microstructure and functional behaviour. *J Mater Res Technol*. 2023;25:6183-6197.

    doi: 10.1016/j.jmrt.2023.06.280

24. Veiga F, Suárez A, Artaza T, Aldalur E. Effect of the Heat Input on Wire-Arc Additive Manufacturing of Invar 36 Alloy: Microstructure and Mechanical Properties. *Weld World*. 2022;66(6):1081-1091.

    doi: 10.1007/s40194-022-01295-4

25. Iturrioz A, Ukar E, Pereira JC. Influence of the manufacturing strategy on the microstructure and mechanical properties of Invar 36 alloy parts manufactured by CMT-WAAM. *Int J Adv Manuf Technol*. 2025;136(2):729-744.

    doi: 10.1007/s00170-024-14853-5

26. Ye S, Xu L, Guo Y, *et al*. Microstructure and mechanical properties of super-invar alloy fabricated by wire-arc additive manufacturing. *Adv Manuf*. Published online February 20, 2025.

    doi: 10.55092/am20250005

27. Jiao G, Fang X, Zhang M, *et al*. Synergistic improvement of mechanical property and thermal expansion of Wire-arc DED Invar alloy enabled by a novel deposition strategy. *J Manuf Process*. 2024;121:121-135.

    doi: 10.1016/j.jmapro.2024.05.031

28. Iturrioz A, Pereira JC, Ukar E. Application of CMT-Twin DED-Arc Process on the Fabrication of Invar 36 by In Situ Alloying. *Materials*. 2025;18(22):5146.

    doi: 10.3390/ma18225146

29. Mattera G, Manoli E, Nele L. Study on the printing stability of Invar 36 alloy under different process parameter conditions in gas metal arc additive manufacturing. *Mater Sci Addit Manuf*. 2025;4(4):025220046.

    doi: 10.36922/MSAM025220046

30. Zhao S, Qiu X, Burnett I, Rigby M, Lele A. A lumped-parameter model for sound generation in gas metal arc welding. *Mech Syst Signal Process*. 2021;147:107085.

    doi: 10.1016/j.ymssp.2020.107085

31. Doodman Tipi AR, Pariz N. Improving the dynamic metal transfer model of gas metal arc welding (GMAW) process. *Int J Adv Manuf Technol*. 2015;76(1):657-668.

    doi: 10.1007/s00170-014-6307-4

32. Teng S, Dehgahi S, Henein H, Wolfe T, Qureshi AJ. Sensor-fusion enabled inter-layer temperature control of nano-treated 7075 aluminum alloy produced through wire-arc directed energy deposition process. *Prog Addit Manuf*. 2025;10(2):1293-1314.

    doi: 10.1007/s40964-024-00707-9

33. Klöpffer W. The critical review of life cycle assessment studies according to ISO 14040 and 14044. *Int J Life Cycle Assess*. 2012;17(9):1087-1093.

    doi: 10.1007/s11367-012-0426-7

34. Acquesta A, Monetta T, Nele L, Mattera G. Process map, microstructure, hardness and corrosion properties of gas metal arc additive manufacturing (GMA-AM) of Invar 36 alloy. *Next Mater*. 2026;11:101839.

    doi: 10.1016/j.nxmate.2026.101839